Influence of acoustic pressure and bubble sizes on the coalescence of two contacting bubbles in an acoustic field

Junjie Jiao[1, 2], Yong He[1]*, Kyuichi Yasui[3], Sandra E. Kentish[4], MuthupandianAshokkumar[2#], Richard Manasseh[5] and Judy Lee[4]*

[1]Department of Mechanical Engineering, Nanjing University of Science and Technology, Jiangsu, China

[2]Particulate Fluids Processing Centre, School of Chemistry, University of Melbourne, Parkville, VIC. 3010 Australia ([#]Adjunct Professor, Chemistry Department, King Abdulaziz University, Jeddah, Saudi Arabia)

[3]National Institute of Advanced Industrial Science and Technology (AIST), 2266-98 Anagahora, Shimoshidami, Moriyama-ku, Nagoya 463-8560, Japan

[4]Particulate Fluids Processing Centre, Chemical and Biomolecular Engineering, University of Melbourne, Parkville, VIC, 3010 Australia

[5]Mechanical and Product Design Engineering, Faculty of Science, Engineering & Technology, Swinburne University of Technology, Hawthorn, VIC, 3122, Australia

***Corresponding Authors**

yhe1964@mail.njust.edu.cn; Tel: +86-25-84315790

jytlee@unimelb.edu.au; Tel: +61-03-9035 8575

Abstract

In this study, the coalescence time between two contacting sub-resonance size bubbles was measured experimentally under an acoustic pressure ranging from 10 kPa to 120 kPa, driven at a frequency of 22.4 kHz. The coalescence time obtained under sonication was much longer compared to that calculated by the film drainage theory for a free bubble surface without surfactants. It was found that under the influence of an acoustic field, the coalescence time could be probabilistic in nature, exhibiting upper and lower limits of coalescence times which are prolonged when both the maximum surface approach velocity and secondary Bjerknes force increases. The size of the two contacting bubbles is also important. For a given acoustic pressure, bubbles having a larger average size and size difference were observed to exhibit longer coalescence times. This could be caused by the phase difference between the volume oscillations of the two bubbles, which in turn affects the minimum film thickness reached between the bubbles and hence the film drainage time. These results will have important implications for developing film drainage theory that to account for the effect of bubble translational and volumetric oscillations, bubble surface fluctuations and microstreaming.

1. Introduction

Bubble coalescence has been extensively studied in the absence of an acoustic field. The coalescence process is divided into three steps[1,2] (see Figure 1(a)): the first step is the contact of the two bubbles to form an initial thin liquid film between them. The second step is thinning of the liquid film to a dimension of about 10^{-6} cm. The third step involves rupture of the film at a dimple point, followed by a rapid coalescence. These three steps are complicated processes which have been extensively studied[3-9] and have been shown to be sensitive to effects such as the approach velocity[7,10-12], the force between the bubbles [13-15] and the fluid viscosity[10,16-19].

The effect of approach velocity is reflected in the Weber (W) number (Eq. 1), which can be used to predict whether two approaching bubbles may coalesce.

$$W = \rho U^2 R_{eq}/\sigma \qquad (1)$$

ρ is the liquid density, U is the velocity of approach, σ is the surface tension and R_{eq} is the equivalent radius of the bubbles, defined as in Eq. 2[7]:

$$\frac{2}{R_{eq}} = \frac{1}{R_1} + \frac{1}{R_2} \qquad (2)$$

where R_1 and R_2 are the radii of the two approaching bubbles. If W < 0.18, the two bubbles will coalesce. Conversely, if the velocity of approach is too fast, W > 0.18, the bubbles will rebound and not coalesce [7] . Kirkpatrick[12] approximated the coalescence (or film drainage) time for free surfaces (in the absence of surface active solute) by using Eq. 3:

$$t_{Ds} \approx R_f \sqrt{\frac{\rho R_{eq}}{16\sigma}} \ln\left(\frac{h_o}{h_c}\right) \qquad (3)$$

where R_f is the radius of the contacting area, h_o is the initial film thickness and h_c is the critical film thickness at which the film ruptures (see Figure 1(b)). The initial and critical thickness of this film has been reported[2] to be in the range of 1 - 10 μm and 0.01 μm, respectively.

If surface active solutes are present at a sufficient surface concentration, the interface could be considered to be immobile (no-slip)[2,4,20] and Eq. 4 is then used to approximate the drainage time[21]:

$$t_{Dn} \approx \frac{3\eta R_{eq} R_f^2}{8\sigma h_c^2} \tag{4}$$

where η is liquid dynamic viscosity.

When bubbles are subjected to an acoustic field, the coalescence process is further complicated by the Bjerknes forces exerted on the bubbles. Depending on their size, bubbles can be drawn towards each other by both primary and secondary Bjerknes forces, with the latter force being dominant at close ranges[22]. The secondary Bjerknes force can also cause the bubbles to repel each other, if the oscillations of the two bubbles are strongly antiphase[23,24]. Details regarding the theoretical calculation of the secondary Bjerknes force were provided by Doinikov[25-27] and in our previous reports[22,28]. The time averaged secondary Bjerknes force (F_B) is related to the average volume oscillation of two bubbles within one acoustic cycle $\langle \dot{V}_1 \dot{V}_2 \rangle$ and is described by Eq. 5[25]:

$$F_B = \langle F_{12} \rangle = \frac{\rho}{4\pi r_{12}^2} \langle \dot{V}_1 \dot{V}_2 \rangle = \frac{4\pi\rho}{r_{12}^2} \langle R_1^2 \dot{R}_1 R_2^2 \dot{R}_2 \rangle \tag{5}$$

where r_{12} is the separation distance between the two bubbles (taken from the center of the bubbles), and the over-dot denotes the time derivative. Eq. 5 shows that the volume change in one acoustic cycle is related to the changes in both radii of the two bubbles (R_1 and R_2) and their radial velocities ($\dot{R}_1$ and $\dot{R}_2$).

Theoretical studies have assumed if two bubbles are drawn together by Bjerknes forces, they will coalesce at encounter[29,30]. There are a few studies on bubble coalescence in an acoustic field. Lee et al.[31] used a total bubble volume method, which stems from the same principle as that reported by Labouret et al.[32], to examine the effect of surface-active solutes on bubble coalescence in the presence of ultrasound (multibubble cavitation). Sunartio et al.[33] and Browne et al.[34] extended the study to investigate various frequency, power, and water-soluble additives on bubble coalescence. However, these studies were performed under multi-bubble systems and

at frequencies where coalescence between bubbles would be difficult to image. In order to understand the role of the secondary Bjerknes force on bubble coalescence, there is a need to study the coalescence of two isolated bubbles in an acoustic field. Crum[35] reported that coalescence of bubbles is normally observed under the influence of Bjerknes forces in a stationary wave field. However, Duineveld[36] demonstrated that this was not always the case and found when two equal size bubbles are driven near resonance, coalescence is inhibited. This was attributed to Bjerknes force induced bubble oscillations causing the contacting surfaces to fluctuate too fast for coalescence to take place. This was further substantiated by the Weber number, which was calculated to be near the critical value of 0.18. In a more recently study, Postema et al.[21,37] investigated the coalescence of lipid coated ultrasound contrast agent bubbles in an acoustic field. They showed that some bubbles bounce off each other, while others show very fast coalescence during bubble expansion caused by the rupturing of the lipid shell to expose the clean bubble surface. This was supported by a good agreement between the experimental coalescence time and that calculated using Eq. 3 for free bubble surface. These studies were performed at high frequencies (0.5 MHz and 1.7 MHz) and high acoustic pressures (0.66 - 0.85 MPa) and for small microbubbles (radii < 2.5 μm). It is unclear whether secondary Bjerknes force played a role, or perhaps was insignificant under the high frequency conditions studied.

It has been shown both experimentally and theoretically that at low acoustic frequencies the magnitude of the secondary Bjerknes force is strongly affected by the size of the two approaching bubbles [22,23,28]. This study aims to compare variations in the secondary Bjerknes forces calculated theoretically to the experimentally measured film drainage time for two bubbles driven at an acoustic frequency of 22.4 kHz and acoustic pressures from 10 kPa to 120 kPa.

2. Experimental and Theoretical Methods

2.1 Experimental method

The details of the experiment setup used to study the bubble coalescence process were described in our previous report[38]. A transducer (American Piezo Ceramics Inc. Z7) was driven at 22.4 kHz by a frequency generator (HM8131-2) coupled to a power amplifier (Krohn-Hite 7500). The

bubble images were magnified using a long-distance microscope, and recorded using a high-speed video camera (Y4-PIV, IDT) at a frame rate of 4000 frames per second. The acoustic pressure was measured using a needle hydrophone (Precision Acoustics Ltd., 1.0 mm needle with preamp). The acoustic pressure used in this study ranged from 10 kPa to 120 kPa. The bubbles were injected via a syringe needle and the coalescence of bubble pairs was recorded and analysed frame by frame using a public domain NIH Image program (developed at the U.S. National Institutes of Health and available on the Internet at http://rsb.info.nih.gov/nih-image/ [date last viewed 11/12/13]). Figure 2 shows a selection of images obtained for a pair of bubbles driven at an acoustic pressure of 30 kPa and 120 kPa. The images illustrate the initial approach of the two bubbles, followed by contact. These images were used to determine R_f and drainage time. It is assume that R_f is the radius of the contacting film, which appears to remain constant during drainage, consistent with that reported by Postema et al. [21]. The drainage time was measured as the time from the point of contact (Frame 4 in Figure 2(a)) until the two bubbles coalesced into one bubble (Frame15 in Figure 2(a)).

2.2 Drainage time in the absence of ultrasound

Eq. 3 and 4 were used to calculate the theoretical drainage time in the absence of ultrasound to compare with the experimental drainage time in the presence of ultrasound. It will not be possible to determine the coalescence of two bubbles using the same system because if the sound field were switched off, the bubbles will rise to the surface under Stokes Law. Due to the limited resolution of the camera, it was not possible to measure the initial and critical film thickness. The initial film thickness (h_o) has been reported[2] to be in the range 1 - 10 μm. Since the bubble radii in this study were in the range 14-32 μm, the lower range of initial film thickness of 1 μm was used in the calculations. The critical film thickness (h_{crit}), has been reported[2] to be approximately 0.01 μm and so this value was used.

2.3 Secondary Bjerknes force for two contacting bubbles.

Eq. 5 assumes the nonlinear convective terms are small. However, for two contacting bubbles, the nonlinear term $\rho w_1 \frac{\partial w_1}{\partial r}$, where w_1 is the radial component of velocity in the liquid created by a bubble, cannot be omitted in the calculation of respective pressure fields, because both w_1 and $\frac{\partial w_1}{\partial r}$ are significant in magnitude. Therefore the equation of liquid motion for two contacting bubbles is thus:

$$\rho \frac{\partial w_1}{\partial t} + \rho w_1 \frac{\partial w_1}{\partial r} + \frac{\partial p_1}{\partial r} = 0 \qquad (6)$$

where, w_1 is the velocity field, r is radial coordinate and p_1 is the pressure in the liquid emitted by the first bubble. The pressure gradient and pressure would then be:

$$\frac{\partial p_1}{\partial r} = -\frac{\rho}{r_{12}^2}\frac{d}{dt}\left(R_1^2 \dot{R}_1\right) + \frac{2\rho R_1^4 \dot{R}_1^2}{r_{12}^2}, \qquad (7)$$

The secondary Bjerknes force* for two contacting bubbles is thus:

$$F_{12} = V_2 \frac{\rho}{r_{12}^2}\frac{d}{dt}\left(R_1^2 \dot{R}_1\right) - 2V_2 \frac{\rho}{r_{12}^2}\left(R_1^4 \dot{R}_1^2\right) \qquad (8)$$

When two bubbles are attached, the bubble-bubble interaction on the bubble pulsation needs to be accounted for and the pressure of an acoustic wave radiated by the first bubble becomes:

$$p_1 = \frac{\rho}{r_{12}^2}\frac{d}{dt}\left(R_1^2 \dot{R}_1\right) - \frac{\rho R_1^4 \dot{R}_1^2}{2r_{12}^2} \qquad (9)$$

This pressure is taken into account in the pulsation of the second bubble by the addition of $\frac{R_1^4 \dot{R}_1^2}{2r_{12}^2}$ to the right side of Eq. 7 in reference[23] to give:

$$\left(1-\frac{\dot{R}_2}{c}\right)R_2\ddot{R}_2 + \frac{3}{2}\dot{R}_2^{\,2}\left(1-\frac{\dot{R}_2}{3c}\right) = \frac{\dot{y}^2}{4} + \left(1+\frac{\dot{R}_2}{c}\right)\frac{p_{sc}}{\rho} + \frac{R}{\rho c}\dot{p}_{sc} - \left(\frac{\rho}{r_{12}}\frac{d}{dt}(R_1^2\dot{R}_1) - \frac{\rho R_1^4 \dot{R}_1^2}{2r_{12}^4}\right) \qquad (10)$$

* Note equations 7 and 8 are time-dependent equations, different to equation 5 which is time-averaged force. F_{21} was also evaluated and the difference were found to be less than 8% .

$$p_{sc} = \left(p_0 + \frac{2\sigma}{R_{20}} \right) \left(\frac{R_{20}}{R_2} \right)^{3\kappa} - p_0 - \frac{2\sigma}{R_2} - \frac{4\mu}{R_2} \dot{R}_2 - P_{ex} \qquad (11)$$

$$P_{ex} = P_a \sin(\omega t) \cos(kd) \qquad (12)$$

where R_{20} is the equilibrium bubble radius of the second bubble. Since the images captured were not performed using a stroboscopic light, the experimental size measured corresponds to the maximum bubble size. The difference between the maximum and equilibrium bubble radius can become significant for acoustic pressures above 60 kPa. Therefore, the equilibrium radius which results in the experimentally observed maximum radius at a given pressure amplitude was determined and used in the secondary Bjerknes force calculations.

The separation distance between two contacting bubbles, r_{12}, is taken as the sum of the experimental radii. Unless otherwise specified, the liquid density and surface tension used were 998 kg/m^3 and 0.072 N/m, respectively[21].

3. Results and Discussion

Plotted in Figure 3 is the measured initial radius of the contacting film between two bubbles (R_f) as a function of the equivalent bubble radius (R_{eq}) calculated using Eq. 2, for acoustic pressures ranging from 10 to 120 kPa. There appears to be a linear relationship between R_f and R_{eq}, irrespective of the applied acoustic pressure. By fitting the data with a linear regression, forced to pass through zero, a slope of approximately 0.68 was obtained. This correlation is in good agreement with the empirical relationship of $R_f = 2/3R_{eq}$ obtained by Postema et al.[21,39] for bubbles generated after a fission event. Although fission and coalescence are different, the relationship represents the contact area formed between bubbles of different sizes.

Replacing R_f with 2/3 R_{eq} in Eq. 3 results in the drainage time being proportional to $R_{eq}^{3/2}$ in the absence of an acoustic field. Postema et al.[21,39] have shown for their lipid shell microbubbles that the drainage time observed is consistent with Eq. 3 for a free bubble surface, despite the microbubbles being coated with a lipid shell. It was argued that during coalescence, the shell ruptured exposing the clean free bubble surface. However, in the present study the experimental

drainage time for two uncoated bubbles is found to be significantly longer compared to that calculated by Eq. 3 for all acoustic pressures (Figure 4). Although in this study the bubbles are driven below resonance, similar inhibition in coalescence to that reported by Duineveld[36] for two equal size bubbles driven near resonance was observed.

Although fresh water was obtained from a Milli-Q water filtration system for all experiments, no stringent measures were taken to eliminate contamination by dust in the air during the experiment. It is unlikely that contamination by dust or the presence of any other surface active impurities could have caused the bubbles to be coated with a rigid layer. In addition, the coalescence process was captured at a frame rate of 0.25 ms per frame. Therefore, any errors arising from determining the initial contact and final coalescence time would be negligible compared to the drainage time measured, which is between 0.002 to 1.03 s. Nevertheless, if Eq. 4 is used, which assumes a rigid no-slip surface, the calculated drainage time appears to estimate the upper boundary of the experimental drainage time. This suggests that the oscillation of the bubbles' surface is inhibiting bubble coalescence to the same extent as that of a surfactant coated bubble.

Even though Postema et al.[21,39] were able to show a good agreement in their observed coalescence time with that calculated using the film drainage theory obtained in the absence of ultrasound, their system is vastly different to that used in this study and that conducted by Duineveld[36]. In their system, the bubbles were coated with a lipid layer and with sizes much smaller (radius less than 2.5 μm) and with a much higher acoustic frequencies (0.5 MHz and 1.7 MHz). In the present study, the bubble radii investigated are much larger and fluctuations in the oscillation amplitude of the bubbles would be considerably greater compared to the bubbles studied by Postema et al.[21,39]. This suggests that the Bjerknes forces would be much stronger in the present study compared to the system conducted by Postema et. al.[21,39]. Similarly, Duineveld [36] studied bubbles with radius between 0.5 to 2 mm, driven near resonance and at a pressure to induce observable Bjerknes effect.

Kirkpatrick and Lockett[12] reported a correlation between coalescence time and surface approach velocity. The film drainage time was plotted against the secondary Bjerknes force and maximum surface approach velocity, shown in

Figure **5** (a) and (b), respectively. To determine the maximum approach velocity, dR_1/dt and dR_2/dt, was calculated as a function of time for one acoustic cycle. This maximum value is assumed to reflect the pressure of the liquid film, i.e. when the maximum approach velocity is large, the pressure of the liquid film between the two bubble walls will be high according to the Bernoulli's equation, resulting in a thicker film and longer drainage time. The secondary Bjerknes forces were calculated using Eq.8 for bubble size R_{10} and R_{20}. Although the data appear scattered, this could be attributed to the influence of bubble-bubble interactions on the critical film thickness for rupture, thus causing the coalescence time to be a probability process with a distribution of values. Shown in

Figure **5** are lines depicting the upper and lower limits of film drainage time, and it does appear that the drainage time increases with both the maximum surface approach velocity and the secondary Bjerknes force. This is in agreement with literature reports relating surface approach velocity and bubble volume oscillations on bubble coalescence[12,36]. For acoustic pressures above 60 kPa, there are limited data to confidently determine the upper and lower boundaries. In addition, at the higher driving pressures of 100 kPa and 120 kPa, shape mode oscillations of bubbles were observed (Figure 2b) which may cause the film drainage time to behave differently to lower acoustic pressures. This probabilistic nature has been reported by Yasui et al[40] for the study on bubble-bubble interaction on destruction of encapsulated microbubbles under ultrasound.

Another possible cause of the variation observed in the data for a given acoustic pressure could be the differences in the size of bubbles. In the study reported by Duineveld[36], the bubbles were of equal size and oscillating in-phase with the same approach velocity. In the present case, some systems have unequal bubble sizes and would be oscillating out of phase. The effect this has on the coalescence time is illustrated in Figure 6, which is a plot of R_{10} verses R_{20} for each pair of bubbles with the measured coalescence time denoted next to the data. A diagonal line is added to indicate equal size bubbles that will be oscillating in-phase. The data appears to suggest that larger bubbles have longer coalescence time, this is clearly observed in 10 kPa. This effect agrees with Eq. 3 and 4, which indicate coalescence time to be proportional to Req. It is also noticed that for a given pressure, the coalescence time appears to be longer for bubble sizes

further away from the diagonal line (these bubbles will be oscillating out of phase). As mentioned earlier, equal size bubbles oscillating in-phase inhibited coalescence. It is speculated that when bubbles are oscillating out of phase, film drainage time will be further hindered compared to when bubbles are oscillating in-phase. The data shown with unfilled symbols are exceptions to these observations.

The enhancement in film drainage time when bubbles are oscillating out of phase is illustrated in the schematic shown in Figure 7, which depicts the variation in the film thickness as a function of time, neglecting the effect of the finite film thickness on the volumetric oscillation. When bubbles are oscillating in-phase, the film thickness is at a minimum during bubble expansion and at a maximum during compression. However, as the difference in the size of the two bubbles increases, the oscillations become anti-phase. In this case the minimum thickness observed in (a) is no longer achieved and because it is at the minimum thickness that coalescence would occur, one would expect a much longer time for coalescence to take place, which is what was observed.

In a further possible physical explanation, bubble translational and volumetric oscillations or bubble-surface fluctuations has been shown[24,41] to induce microstreaming around the bubble and depending on the flow pattern, microstreaming within the liquid film could contribute towards coalescence inhibition. Furthermore, a recent report by Collis et al.[42] showed what they believed were the first images of the theoretically predicted primary vortices in the boundary layer of the bubble surface, indicating velocities at least an order of magnitude higher than the secondary microstreaming hitherto observed. Thus, as two bubbles get very close, the influence of microstreaming could become significant.

Conclusion

In this study, it was shown that bubbles driven at low frequencies exhibit much longer coalescence times compared to that calculated by the film drainage theory developed in the absence of ultrasound. These coalescence times were comparable with that predicted for rigid

(surfactant coated) bubbles, even in the absence of surfactant. This suggests that the film drainage theory developed in the absence of ultrasound do not fully describe the coalescence process for two coalescing bubbles undergoing volume oscillations. The results are suggesting that the coalescence process could be statistical, with a distribution of film drainage times which increase with increasing surface approach velocity and secondary Bjerknes force. Furthermore, bubbles oscillating in and out of phase to each other due to differences in the bubble sizes may influence film drainage time. These findings will be important in understanding bubble coalescence in an acoustic field and for the development of film drainage theory that takes into account the effect of bubble translational and volumetric oscillations, bubble surface fluctuations and microstreaming.

ACKNOWLEDGEMENTS

We are grateful to Prof Yos Morsi for facilitating the use of the high-speed camera. The financial support through the Australian Research Council for the DECRA (Discovery Early Career Research Award, DE120101567) is also gratefully acknowledged.

References

1. Marrucci, G. A theory of coalescence *Chem. Eng. Sci.* **1969**, 24, 975-985.
2. Oolman, T. O.; Blanch, H. W. Bubble coalescence in stagnant liquids *Chem. Eng. Commun*, 43, 237-261.
3. Cain, F. W.; Lee, J. C. A technique for studying the drainage and rupture of unstable liquid films formed between two captive bubbles: Measurements on kci solutions *J. Colloid Interface Sci* **1985**, 106, 70-85.
4. Abid, S.; Chesters, A. K. The drainage and rupture of partiallymobile films between colliding drops at constant approach velocity *Int. J. Multiphase Flow* **1994**, 20, 613-631.
5. Ida, M. P.; Miksis, M. J. Thin film rupture *Appl. Math. Lett.* **1996**, 9, 35-40.
6. Chen, L.; Li, Y.; Manasseh, R. In Third International Conference on Multiphase Flow: Lyon, France, 1998, p 1-8.
7. Duineveld, P. C. Bouncing and coalescence of bubble pairs rising at high reynolds number in pure water or aqueous surfactant solutions *Appl. Sci. Res* **1998**, 58, 409-439.
8. Chen., R. H.; Tian, W. X.; Su, G. H.; Qiu, S. Z.; Ishiwatari, Y.; Oka, Y. Numerical investigation on coalescence of bubble pairs rising in a stagnant liquid *Chem. Eng. Sci* **2011**, 66, 5055-5063.
9. Manasseh, R.; Riboux, G.; Risso, F. Sound generation on bubble coalescence following detachment *International Journal of Multiphase Flow* **2008**, 34, 938-949.
10. Chesters., A. K.; Hofman., G. Bubble coalescence in pure liquids *Appl. Sci. Res* **1982**, 38, 353-361.
11. Hagesæther, L. In Department Of Chemical Engineering; Norwegian University Of Science And Technology: Trondheim Norway, 2002.
12. Kirkpatrick, R. D.; Lockett, M. J. The influence of approach velocity on bubble coalescence *Chem. Eng. Sci* **1974**, 29, 2363-2373.
13. Davis, R. H. The lubrication force between two viscous drops *Phys. Fluids A* **1989**, 1, 77-81.
14. Hartland, S.; Jeelani, S. A. K. Inertial effects in thin film drainage *Chem. Eng. Sci* **1989**, 44, 387-391.
15. Hengel, E. I. V. v. d.; Deen, N. G.; Kuipers, J. A. M. Application of coalescence and breakup models in a discrete bubble model for bubble columns *Ind. Eng. Chem. Res* **2005**, 44, 5233-5245.
16. Hasan, N.; Zakaria, Z. B. Computational approach for a pair of bubble coalescence process *Int. J. Heat Fluid Flow* **2011**, 32, 755-761.
17. Li, D. Coalescence between small bubbles: Effects of surface tension gradient and surface viscosities *J. Colloid Interface Sci* **1996**, 181, 34-44.
18. Li, D. Coalescence between small bubbles: Effects of bulk and surface diffusion *Chem. Eng. Sci* **1996**, 51, 3630-3630.
19. Manev, E. D.; Nguyen, A. V. Effects of surfactant adsorption and surface forces on thinning and rupture of foam liquid films *Int. J. Miner. Process.* **2005**, 77, 1-45.
20. Lin, C. Y.; Slattery, J. Thinning of a liquid film as a small drop or bubble approaches a solid plane *AIChE Journal* **1982**, 28, 147-156.
21. Postema, M.; Marmottant, P.; Lancee, C. T.; Hilgenfeldt, S.; Jong, N. D. Ultrasound-induced microbubble coalescence *Ultrasound Med Biol* **2004**, 30, 1337-1344.
22. Jiao, J.; He, Y.; Leong, T.; Kentish, S. E.; Ashokkumar, M.; Manasseh, R.; Lee, J. Experimental and theoretical studies on the movements of two bubbles in an acoustic standing wave field *J. Phys. Chem. B* **2013**, 117, 12549-12555.
23. Mettin, R.; Akhatov, I.; Parlitz, U.; Ohl, C. D.; Lauterborn, W. Bjerknes forces between small cavitation bubbles in a strong acoustic field *Phys. Rev. E* **1997**, 56, 2924-2930.
24. Tho, P.; Manasseh, R.; Ooi, A. Cavitation microstreaming patterns in single and multiple bubble systems *J. Fluid Mech.* **2007**, 576, 191-233.
25. Doinikov, A. A. Translational motion of two interacting bubbles in a strong acoustic field *Phy. Rev. E* **2001**, 64, 0263011-0263016.

26. Doinikov, A. A. Translational motion of a spherical bubble in an acoustic standing wave of high intensity *Phys. Fluids* **2002**, 14, 1420-1425.
27. Doinikov, A. A.; Zavtrak, S. T. On the mutual interaction of two gas bubbles in a sound field *Phys. Fluids* **1995**, 7, 1923-1230.
28. Jiao, J.; He, Y.; Kentish, S. E.; M. Ashokkumar; Manasseh, R.; Lee, J. Effects of frequency and bubble size on secondary Bjerknes force between two bubbles in a standing wave *Submitted to Journal of Ultrasonics* **2014**.
29. Oguz, H. N.; Prosperetti, A. A generalization of the impulse and virial theorem with an application to bubble oscillations *J. Fluid Mech.* **1990**, 218, 143-162.
30. Pelekasis, N. A.; Tsamopoulos, J. A. Bjerknes forces between two bubbles. Part 2. Response to an oscillatory pressure field *J. Fluid Mech.* **1993**, 254, 501-527.
31. Lee., J.; Kentish., S. E.; Ashokkumar., M. The Effect of Surface-Active Solutes on Bubble Coalescence in the Presence of Ultrasound *J. Phys. Chem. B.* **2005**, 109, 5095-5099.
32. Labouret, S.; Frohly, J. Bubble size distribution estimation via void rate dissipation in gas saturated liquid. Application to ultrasonic cavitation bubble fields *Eur. Phys. J.* **2002**, 19, 39-54.
33. Sunartio., D.; Ashokkumar., M.; Grieser., F. Study of the Coalescence of Acoustic Bubbles as a Function of Frequency, Power, and Water-Soluble Additives. *J. Am. Chem. Soc.* **2007**, 129, 6031-6036.
34. Browne., C.; Tabor., R. F.; Chan., D. Y. C.; Dagastine., R. R.; Ashokkumar., M.; Grieser, F. Bubble Coalescence during Acoustic Cavitation in Aqueous Electrolyte Solutions *Langmuir* **2011**, 27, 12025-12034.
35. Crum, L. A. Bjerknes forces on bubbles in a stationary sound field *J. Acoust. Soc. Am* **1975**, 57, 1363-1370.
36. Duineveld, P. C. The influence of an applied sound field on bubble coalescence *The Journal of the Acoustical Society of America* **1996**, 99, 622-624.
37. Postema., M.; Wamel., A. v.; Lancée., C. T.; Jong., N. d. Ultrasound-induced encapsulated microbubble phenomena *Ultrasound Med Biol* **2004**, 6, 827-840.
38. Jiao, J.; He, Y.; Leong, T.; Kentish, S. E.; Ashokkumar, M.; Manasseh, R.; Lee, J. Experimental and Theoretical Studies on the Movements of Two Bubbles in an Acoustic Standing Wave Field *J. Phys. Chem. B* **2013**, 117, 7.
39. Postema, M.; Marmottant, P.; Lancee, C. T.; Versluis, M.; Hilgenfeldt, S.; Jong, N. D. In International Ultrasonics, Ferroelectrics and Frequency Control Joint 50th Anniversary Conference, 2004, p 1-4.
40. Yasui, K.; Lee, J.; Tuziuti, T.; Towata, A.; Kozuka, T.; Iida, Y. Influence of the bubble-bubble interaction on destruction of encapsulated microbubbles under ultrasound *The Journal of the Acoustical Society of America* **2009**, 126, 973-982.
41. Leong, T.; Collis, J.; Manasseh, R.; Ooi, A.; Novell, A.; Bouakaz, A.; Ashokkumar, M.; Kentish, S. The Role of Surfactant Headgroup, Chain Length, and Cavitation Microstreaming on the Growth of Bubbles by Rectified Diffusion *The Journal of Physical Chemistry C* **2011**, 115, 24310-24316.
42. Collis, J.; Ooi, A.; Manasseh, R. In 17th Australlasian Fluid Mechanics Conference: Auckland, New Zealand, 2010.

Figure Captions

Figure 1: Schematic representation of (a) coalescing process of two colliding bubbles: approach [i–ii], flattening of the interposed film [iii], drainage to a critical thickness and there is a dimple on the film [iv], film rupture [v], and formation of a single bubble [iv], and (b) variables used for two bubble in contact.

Figure 2: Optical image depicting the coalescence process of two bubbles driven at an acoustic pressure of (a) 30 kPa (the bubble radius are 24 μm and 27 μm) and (b) 120 kPa (the bubble radius are 22 μm and 26 μm). The numbers denote the frame number captured at 4000 fps. A small bubble can be seen attached to one of the bubbles from Frame 1 to 10 in (a) and from Frames 1 to 5 in (b). These were sometimes captured, but do not appear to be affecting the trends observed. For 120 kPa, shape mode oscillations can be observed as soon as the two bubbles becomes in contact (Frame 5).

Figure 3: The measured film radius between the two contacting bubbles (R_f) is plotted as a function of the equivalent bubble radius (R_{eq}) calculated using Eq. (2) for pressures ranging from 10 to 120 kPa. The data is fitted with a linear regression, forced to pass through zero, which yields a slope of 0.68.

Figure 4: Drainage time as a function of acoustic pressure. The drainage time in the absence of ultrasound is calculated using Eq. 3 and Eq. 4, using the R_{eq} of 21.1 μm, averaged from all the experimental R_{eq} data ranging from 14.5 to 31 μm. The value of 0.072 N/m was used for surface tension. Note that the y axis for the drainage time is a log scale.

Figure 5: Film drainage time as a function of (a) Secondary Bjerknes force and (b) maximum (dR1/dt + dR2/dt) for different driving acoustic pressures. The lines indicate the upper and lower limits of film drainage time.

Figure 6: A plot of R_{10} vs R_{20} and the corresponding experimental film drainage time, in seconds, is labelled next to the data for different acoustic pressures. The diagonal line denotes when the two bubbles are of equal size, oscillating in-phase. The data appear to show increase in coalescence time as size of the bubble pairs are larger and deviates away from the diagonal line (these bubbles will be oscillating anti-phase). Data exception to this observation is shown as unfilled symbols.

Figure 7: A schematic diagram illustrating the fluctuations in the film thickness for (a) bubbles oscillating in phase and (b) for bubble oscillating out of phase. For each case, the outlines of the bubbles at the maximum and minimum stages are also shown.

Figure 1

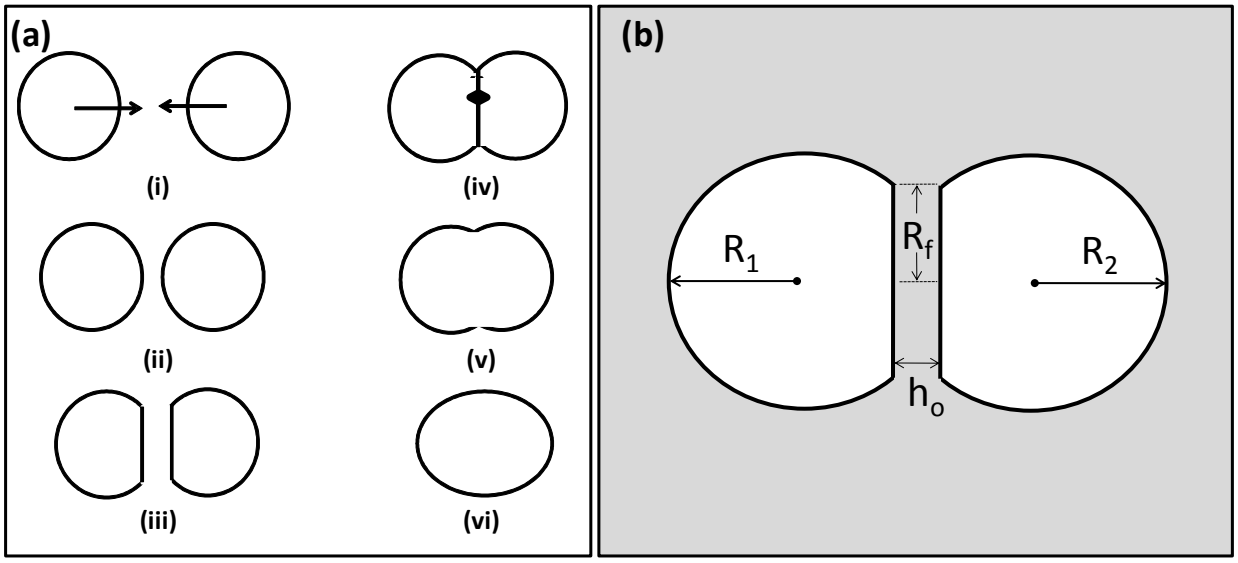

Figure 2

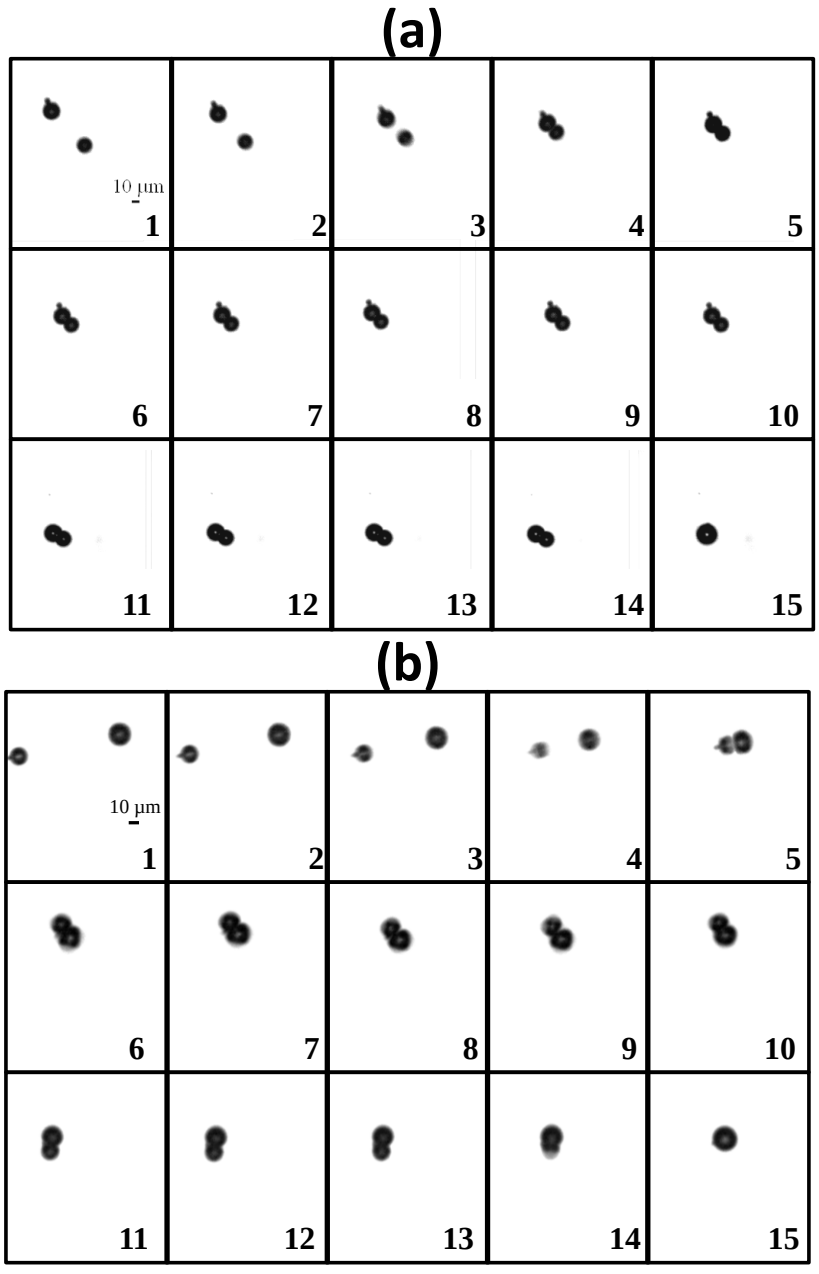
(a)
10 µm
1
2
3
4
5
6
7
8
9
10
11
12
13
14
15
(b)
10 µm
1
2
3
4
5
6
7
8
9
10
11
12
13
14
15

Figure 3

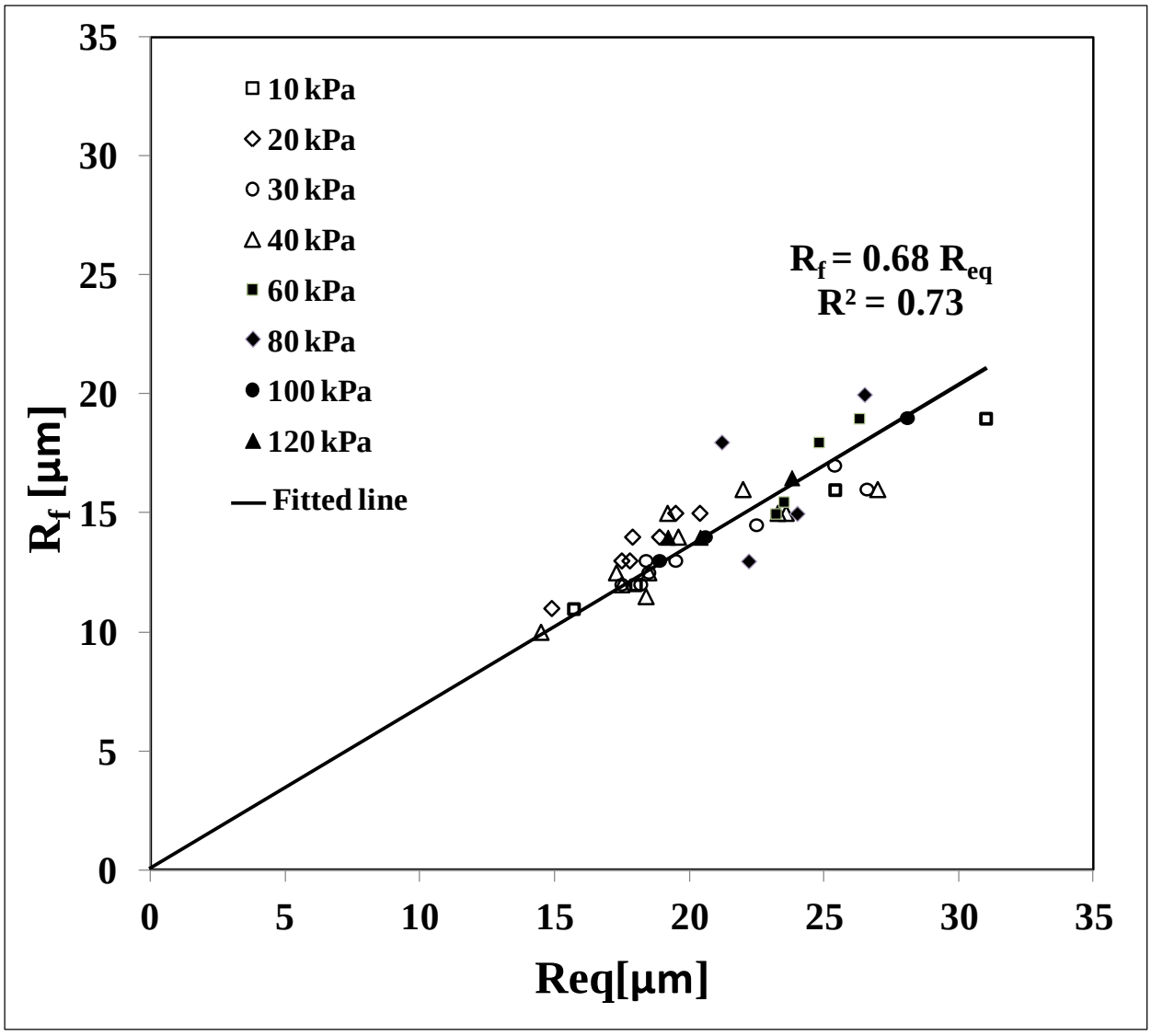
10 kPa
20 kPa
30 kPa
40 kPa
60 kPa
80 kPa
100 kPa
120 kPa
Fitted line
$R_f = 0.68\ R_{eq}$
$R^2 = 0.73$
R_f [µm]
Req[µm]
0
5
10
15
20
25
30
35

Figure 4

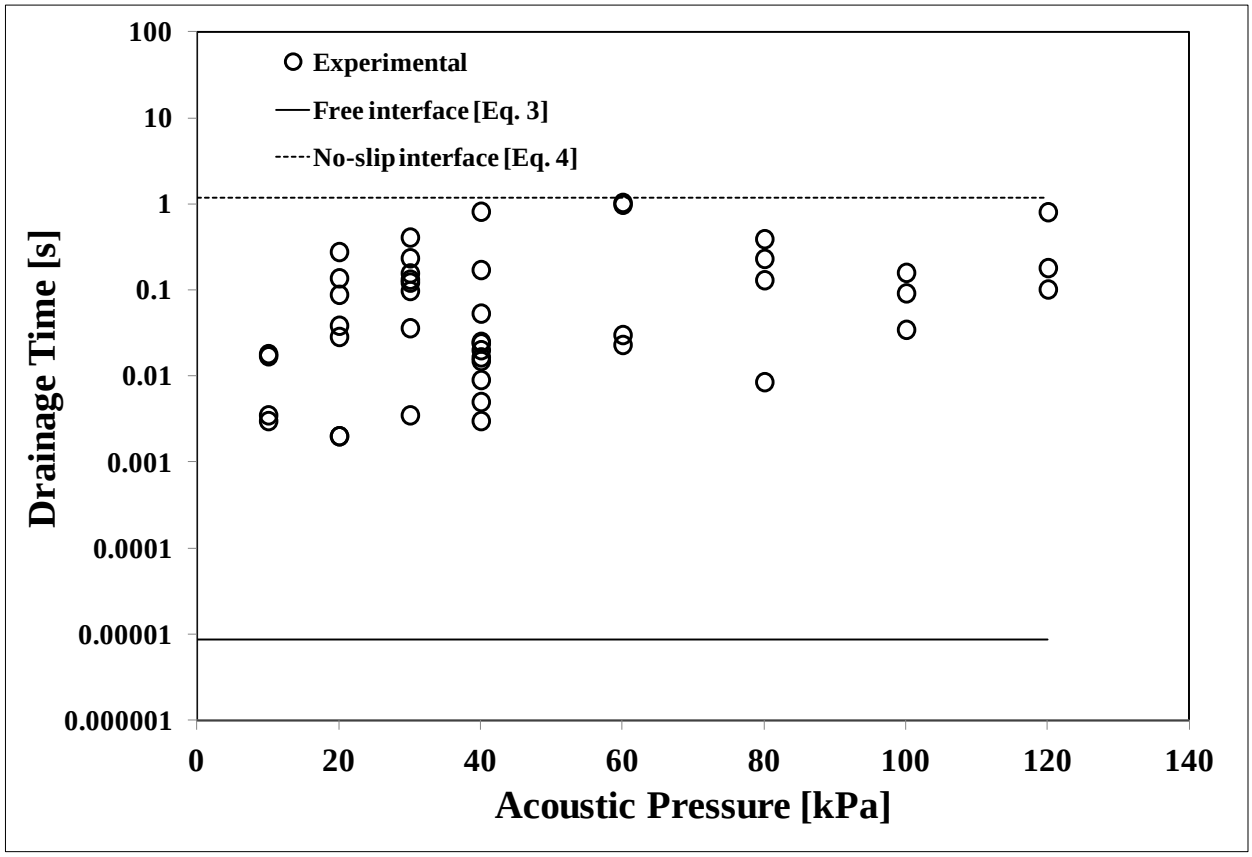
Experimental
Free interface [Eq. 3]
No-slip interface [Eq. 4]
Drainage Time [s]
100
10
1
0.1
0.01
0.001
0.0001
0.00001
0.000001
0
20
40
60
80
100
120
140
Acoustic Pressure [kPa]

Figure 5

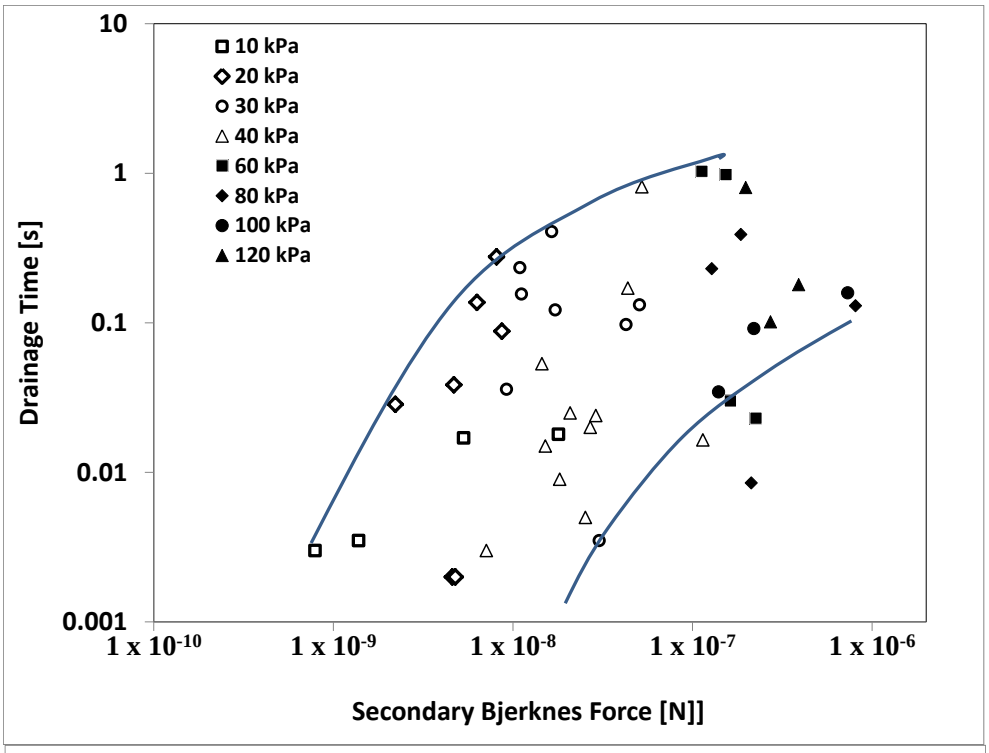
10
1
0.1
0.01
0.001
Drainage Time [s]
10 kPa
20 kPa
30 kPa
40 kPa
60 kPa
80 kPa
100 kPa
120 kPa
1 x 10-10
1 x 10-9
1 x 10-8
1 x 10-7
1 x 10-6
Secondary Bjerknes Force [N]]

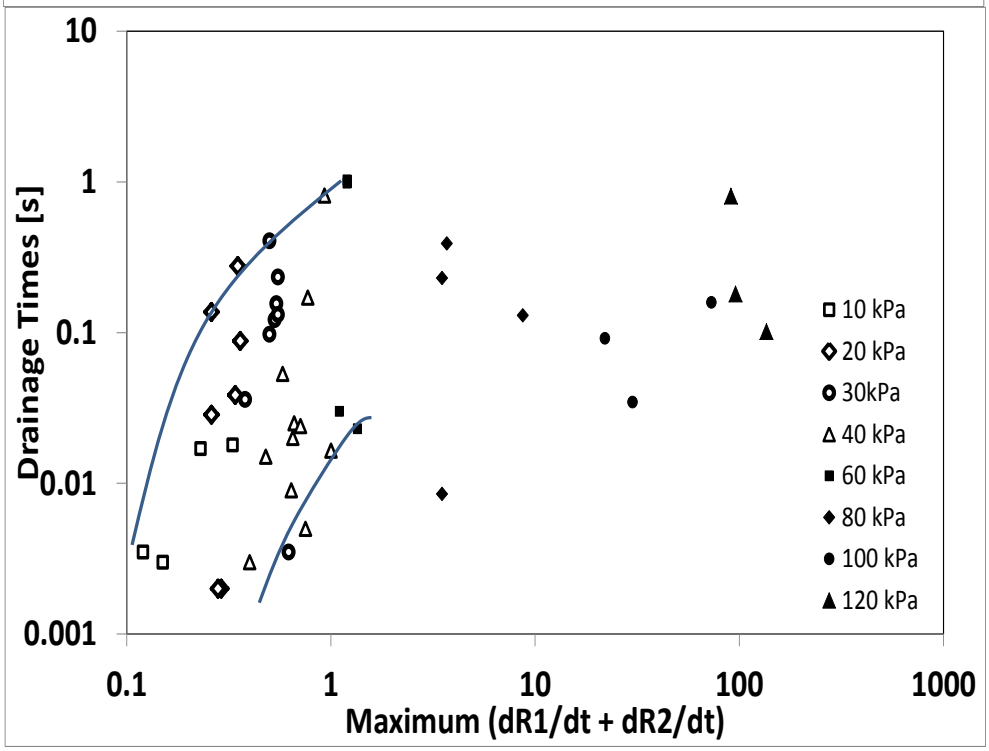
10
1
0.1
0.01
0.001
Drainage Times [s]
10 kPa
20 kPa
30kPa
40 kPa
60 kPa
80 kPa
100 kPa
120 kPa
0.1
1
10
100
1000
Maximum (dR1/dt + dR2/dt)

Figure 6

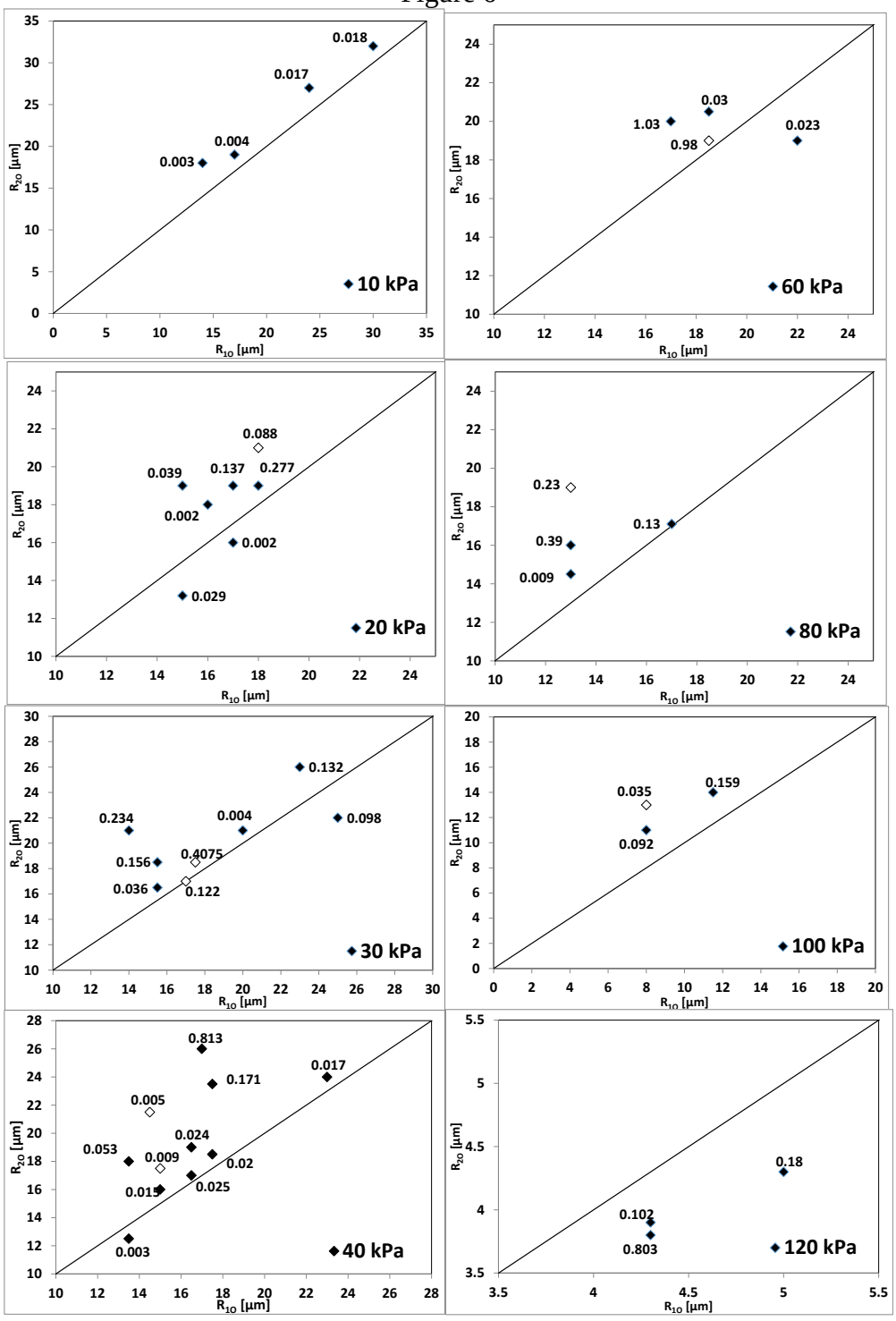
0.018
0.017
0.004
0.003
10 kPa
0.03
1.03
0.98
0.023
60 kPa
0.088
0.039
0.137
0.277
0.002
0.002
0.029
20 kPa
0.23
0.13
0.39
0.009
80 kPa
0.132
0.234
0.004
0.098
0.4075
0.156
0.036
0.122
30 kPa
0.035
0.159
0.092
100 kPa
0.813
0.171
0.017
0.005
0.024
0.053
0.009
0.02
0.015
0.025
0.003
40 kPa
0.18
0.102
0.803
120 kPa
R20 [µm]
R10 [µm]

Figure 7

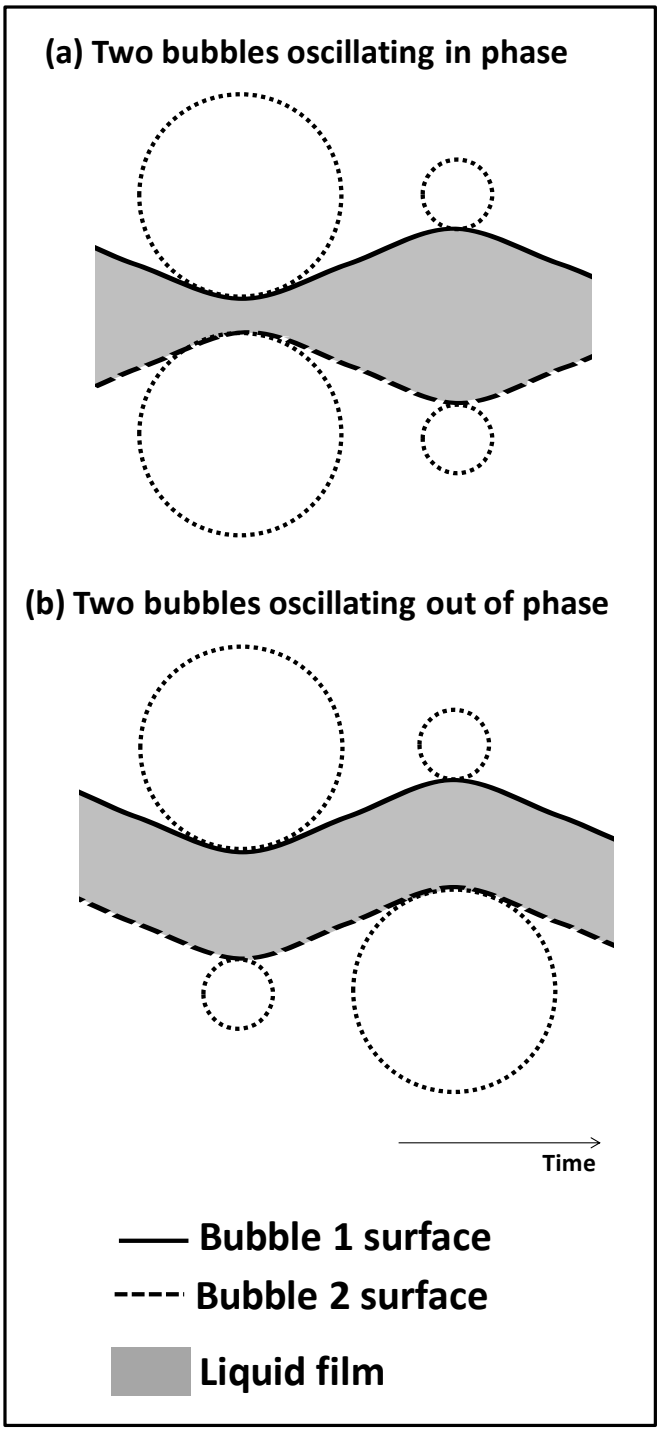
(a) Two bubbles oscillating in phase
(b) Two bubbles oscillating out of phase
Time
Bubble 1 surface
Bubble 2 surface
Liquid film